International Journal of Applied Pharmaceutics

ISSN- 0975-7058 Vol 17, Issue 1, 2025

Original Article

BOX-BEHNKEN OPTIMIZATION OF MELOXICAM MICROCAPSULE SCAFFOLDS FOR PRECISION DRUG DELIVERY IN ARTHRITIS: ENHANCED STABILITY, EFFECTIVE STERILIZATION, AND *IN VIVO* THERAPEUTIC POTENTIAL

SAMPATH KUMAR, MOTHILAL MOHAN*

Department of Pharmaceutics, SRM College of Pharmacy, SRM Institute of Science and Technology, Kattankulathur-603203, Tamil Nadu, India

***Corresponding author: Mothilal Mohan; *Email: mothilam@srmist.edu.in**

Received: 26 Jul 2024, Revised and Accepted: 06 Dec 2024

ABSTRACT

Objective: This study aims to develop and evaluate an innovative implantable drug delivery system using gelatin microspheres loaded with Nonsteroidal Anti-Inflammatory Drugs (NSAIDs), namely meloxicam (MXM), integrated into a gelatin scaffold. This system is designed to enhance drug delivery efficiency and sustain drug release.

Methods: MXM-loaded microspheres with a 1:1 ratio of Poly Lactic Acid (PLA) and Poly Lacto Glycolic Acid (PLGA) were optimized for size, yield, efficiency, and release. Gelatin scaffolds were designed as rod-shaped implants, tested for stability and degradation in pH 7.4 and pH 4.0 buffers at 37 °C for 100 d, and sterilized with γ-radiation. Implants were evaluated in rabbits, with blood samples analyzed via High-Performance Liquid Chromatography (HPLC) for pharmacokinetic parameters statistically analyzed ($P<0.05$).

Results: The microspheres with a 1:1 ratio of PLA and PLGA demonstrated favorable characteristics such as smaller particle sizes, high yield, and efficient drug entrapment and release. Optimization using Design Expert resulted in highly desirable scaffolds, evidenced by a desirability factor close to one across all assessed variables. The scaffolds exhibited robust physicochemical properties, including sustained drug release over an extended period, highlighting their potential for diverse biomedical applications. Implants showed greater stability in pH 7.4 buffer solutions in contrast to pH 4.0 over 100 d, with higher mass loss in acidic environments (14.4% vs. 9.66%). γ-Radiation sterilization effectively prevented microbial contamination. *In vivo* studies confirmed MXM detection in plasma, with Scaffold-MXM microspheres (iS-MMS-17) (optimized implantable scaffold) showing higher mean C_{max} values and significant Area Under Curve (AUC) parameters, suggesting its potential for effective therapy.

Conclusion: The study found that the scaffolds exhibited strong physicochemical properties and sustained drug release, making them suitable for biomedical use. Implants were more stable at pH 7.4 than at pH 4.0, and γ-radiation effectively prevented microbial contamination. *In vivo* studies confirmed MXM detection, with iS-MMS-17 showing promising pharmacokinetic parameters for pain and arthritis therapy.

Keywords: Entrapment, Implants, Microspheres, Meloxicam, Expulsion, Scaffolds

DOI: https://dx.doi.org/10.22159/ijap.2025v17i1.52160 Journal homepage: https://innovareacademics.in/journals/index.php/ijap

INTRODUCTION

Microspheres are a cutting-edge technology in drug delivery, offering significant benefits for the controlled and sustained release of medications. These spherical particles, typically between 1 and 1000 µm, are crafted from biocompatible and biodegradable polymers. They encapsulate drugs, protecting them from degradation, enhancing stability, and allowing precise targeting of specific body sites [1]. This targeted delivery minimizes systemic side effects and boosts therapeutic efficacy. The discharge rate of encapsulated drugs can be finely adjusted by altering the microspheres' composition and structure, enabling extended and controlled drug release over time [2]. Versatile in their administration, microspheres can be delivered orally, as injectable, or as implants, making them suitable for various medical applications, including cancer therapy and chronic disease management [3]. Their ability to give a prolonged and controlled drug delivery enhances patient compliance and improves treatment outcomes, making microspheres a valuable asset in modern pharmaceutical development [4].

Nonsteroidal Anti-Inflammatory Drugs (NSAIDs) are usually recommended for arthritis due to their effectiveness in reducing inflammation and pain. However, when administered orally, NSAIDs often cause significant gastrointestinal side effects, such as ulcers and bleeding, due to their systemic absorption and direct irritation of the stomach lining [5]. To mitigate these adverse effects, transdermal delivery has emerged as a promising alternative. Transdermal NSAID formulations allow the drug to be absorbed through the skin directly into the affected tissues, providing localized pain relief and reducing systemic exposure. This method not only minimizes gastrointestinal risks but also ensures a steady release of medication, leading to more consistent therapeutic effects and improved patient compliance [6]. Consequently, transdermal NSAID delivery offers a safer and potentially more effective treatment option for arthritis patients, addressing both pain management and the limitations of oral administration [7].

Meloxicam (MXM), a potent NSAID in the oxicam class, effectively relieves pain and inflammation associated with arthritis through the inhibition of prostaglandin production [8]. Available in oral tablets, capsules, and injectable solutions, its long duration of action supports once-daily dosing, enhancing patient compliance despite potential side effects like gastrointestinal discomfort and fluid retention [9]. Transdermal delivery of MXM shows promise by providing localized pain relief without systemic effects, leveraging skin barriers for sustained release, and minimizing gastrointestinal irritation. Challenges remain in optimizing formulations for effective skin permeation and consistent drug delivery in chronic pain management [10].

Microspheres embedded in scaffolds represent a sophisticated approach to drug delivery, combining the advantages of controlled release systems with the structural support of scaffolds [11]. These microspheres, typically composed of biodegradable polymers, encapsulate drugs and are integrated into porous scaffolds designed to mimic the extracellular matrix. This combination facilitates sustained and localized drug release, protecting the drug payload from degradation and ensuring precise delivery to target tissues [12]. The porous nature of the scaffold allows for cell infiltration and tissue integration, promoting therapeutic efficacy in reformative medicine and tissue engineering applications. This approach holds

promise for treating various conditions by tailoring drug release kinetics and enhancing tissue regeneration while minimizing systemic side effects [13].

This investigation aimed to fabricate aggregate MXM microspheres using the solvent evaporation method. These microspheres were subsequently incorporated into gelatin scaffolds to achieve sustained topical drug delivery for long-term arthritis therapy. Gelatin scaffolds containing co-encapsulated microspheres were optimized using the Box-Behnken Design (BBD).

MATERIALS AND METHODS

Materials

MXM was generously provided as a gift sample by Micro Labs Limited, Bangalore, India. Gelatin, acetic acid, hydrochloric acid, glycerol, Poly Lactic Acid (PLA), Poly Lacto Glycolic Acid (PLGA), sorbitol, ethanol, and vegetable oil were obtained from qualigens, India, and local suppliers. Merck chemicals delivered acetonitrile, o-phosphoric acid, and HPLC-grade water.

Making of MXM-loaded microspheres

In the experiment, 9 microsphere batches were made using different ratios of MXM to polymer. Two distinct polymers, PLGA and PLA, were employed. The formulations i. e., MXM Microspheres (MMS) were named as MMS-1 to MMS-9 (table 1). The production process involved dissolving the MXM and polymers (equal proportions of PLGA and PLA) in the designated proportions at room temperature. An equimolar proportion of ethanol and dichloromethane is used as a solvent to dissolve. Vigorous agitation was applied to ensure homogeneous dispersion of the MXM and polymer. Subsequently, this mixture was introduced slowly into a dispersion medium comprising 50 ml of heavy liquid paraffin along with 1.5% span 80. An overhead propeller agitator was employed at 400 rpm to stir the system at room temperature for 2-3 h. This duration allowed for the complete evaporation of the solvent. Following this step, the liquid paraffin was separated, and the resulting microspheres were isolated by filtration using a Whatman filter paper. To purify the microspheres, they were washed three times using 180 ml of acetone. Afterward, the microspheres were air-dried for 24 h [14-16].

Table 1: Various MXM microspheres formulae

Formulation	MXM: Polymer (ratio)	MXM (mg)	PLGA (mg)	PLA (mg)	DCM (ml)	Methanol (ml)	Liquid paraffin (ml)
MMS-1	1:0.25	10	2.50	2.50	15	10	200
MMS-2	1:0.5	10	5.00	5.00	15	10	200
MMS-3	1:0.75	10	7.50	7.50	15	10	200
MMS-4	1:1.00	10	10.00	10.00	15	10	200
MMS-5	1:1.25	10	12.50	12.50	15	10	200
MMS-6	1:1.50	10	15.00	15.00	15	10	200
MMS-7	1:1.75	10	17.50	17.50	15	10	200
MMS-8	1:2.00	10	20.00	20.00	15	10	200
MMS-9	1:2.25	10	22.25	22.25	15	10	200

MMS: MXM microspheres; DCM: Dichloromethane

Based on the evaluation of key parameters such as production yield, Encapsulation Efficiency (EE), and *in vitro* MXM release, MMS-4 demonstrated superior performance, establishing it as the optimal candidate for subsequent scaffold production.

Measuring the physical and drug expulsion possessions of microspheres

Compatibility studies

The compatibility and interfaces of MXM with the excipients used were evaluated through the following methods:

Differential scanning calorimetry (DSC) observations

In DSC studies, initial baseline analyses are conducted individually on MXM and each excipient to establish their respective thermal profiles. Subsequently, physical mixtures containing MXM and all excipients are prepared and analyzed to detect any changes in thermal behavior, such as shifts in peak temperatures, emergence of new peaks, or alterations in enthalpies. These observations help identify potential interactions or incompatibilities between MXM and the excipients. Solid-state compatibility is further assessed to ascertain crystallinity, amorphousness, or any polymorphic transformations that may occur.

Fourier transform infrared (FTIR) spectroscopic observations

The FTIR spectroscopy analysis spanned from 400 to 4000 cm^{-1}, covering a wide range of infrared frequencies that correspond to molecular vibrations and bonds. Five trials were conducted, and the mean spectra were evaluated to enhance the signal-to-noise ratio, providing valuable insights into the molecular composition and structure of the samples.

Measuring the physical and drug expulsion possessions of MXM microspheres

The following tests were conducted for the MXM microspheres:

Scanning electron microscopy (SEM) analysis

The assessment of physical properties included determining the Particle Size (PS) of the microspheres and analyzing their surface morphology using SEM. The PS measurements were conducted by placing dry microspheres on a clean glass slide and employing stage micrometers for accuracy. Subsequently, SEM analysis provided detailed images of the microsphere surfaces [17].

Yield

The production yield (Y) of the microspheres was assessed by dividing the average weight of microspheres recovered from each of the three trials (W_1) by the total weight of the initial dry material used (W_2), and then multiplying by 100 to express it as a percentage. This scheming provided insight into the efficiency of the microsphere production process, reflecting how much of the initial material was positively converted into microspheres [18]. The resulting yield percentage helped assess the effectiveness and reproducibility of the manufacturing process, crucial for scaling up production and ensuring consistent quality of the microsphere formulations (e. q.1).

$$\%Y = \frac{W1}{W2} X100 \text{--- (1)}$$

Entrapment efficiency

In a solution of 0.1 M HCl, 100 mg of microspheres were dispersed overnight with periodic agitation. Following this, the mixture was clarified, and the filtrate was subjected to spectrophotometric analysis at 360 nm. The EE was calculated by determining the ratio of the actual amount of MXM in the formulation to the initially added quantity [19]. This assessment provided a measure of how effectively the microspheres encapsulated the intended drug, crucial for evaluating their performance as drug delivery systems (e. q.2).

$$\%EE = \frac{\text{Practical drug yield}}{\text{Theoritical MXM content}} X\ 100 \text{ --- (2)}$$

In vitro MXM expulsion calculation

The dissolution properties of the microspheres were investigated using the USP-II apparatus under controlled conditions: operating at 50 rpm and keeping at 37±0.5 °C with 900 ml of 0.1N HCl as the dissolution medium. Samples of 5 ml were withdrawn at specified

intermissions, and the dissolution medium was replenished accordingly. Analysis of the withdrawn samples was performed spectrophotometrically at 360 nm. Following a thorough evaluation, MMS-4 was identified as the most suitable candidate for scaffold fabrication due to its favorable dissolution behavior and overall performance attributes [20].

Making of MMS-loaded gelatin scaffold

The optimized formulation, MMS-4, was subsequently chosen for scaffold production using Design Expert (Version 11) software.

Experimental design

In this study, Design Expert Software was adopted to optimize the formulation variables of Scaffold Microspheres (SMSs). This study exploited the BBD to assess the impact of various factors, viz., gelatin level [-1] (800 mg), [0] (900 mg), and [+1] (1000 mg) as (X_1), propylene glycol [-1] (0.6 ml), [0] (0.75 ml), and [+1] (0.9 ml) as (X_2), and the freezing time of the scaffold [-1] (10 min), [0] (15 min), and [+1] (20 min)] (X_3), on the responses: the EE of MXM (Y_1) and the expulsion of MXM (Y_2). ANOVA and statistics were used to find lack-of-fit tests, and the outcomes were thoroughly analyzed. The model selection process involved comparing the PRESS (Prediction Residual Sum of Squares) values among the suggested models, ultimately choosing the one with the lowest PRESS as the best-fitting model for the data [21, 22]. This comprehensive approach provided appreciated insights into the relationships between the variables and the responses of interest, contributing to the optimization of SMS formulations (table 2).

Table 2: Composition of different S-MMSs by BBD

Independent variables	Levels		
	Low	Medium	High
X_1= Gelatin (mg/100 ml)	800	900	1000
X_2= Propylene glycol (mg/100 ml)	0.6	0.75	0.9
X_3= Freezing Time (min)	10	15	20
Changed values	-1	0	+1
Dependent variables	Criteria		
Y_1= EE	Maximize		
Y_2= Drug release	Maximize		

The dispensation of the MMSs-loaded scaffolds

The preparation of the MXM microspheres-loaded gelatin scaffolds involved several sequential steps. Initially, gelatin powder was completely dissolved in deionized water at 40 °C. Glycerin and sorbitol were added to the gelatin solution, followed by thorough mixing to achieve uniformity and consistency. Subsequently, the prepared solution was carefully injected into a mold, ensuring the prevention of bubble formation throughout the process [23].

The gel formation began by placing the mold at 4 °C for 1 h, followed by gradual cooling to-20 °C and subsequently to-80 °C. Once fully frozen, the gelatin matrix underwent freeze-drying, resulting in the formation of a scaffold structure.

Design Expert Software was instrumental in designing the compositions of various scaffold formulations, as detailed in table 2. Before optimization, twenty distinct formulations were prepared based on the software's recommendations. For the optimized formulation, Scaffold-MXM Microspheres (SMMSs) were prepared. Glutaraldehyde served as a cross-linker in the fabrication of these microspheres, which were then incorporated into the gelatin scaffold. This intricate process followed a series of controlled steps to ensure the successful progress of the MXM-loaded gelatin scaffold, aligned with the experimental design and optimization facilitated by the software [24].

Evaluation of MXM microspheres loaded scaffolds

EE of MXM in MXM microspheres and its scaffolds

Approximately a 1-inch scaffold was dissolved in a 25 ml phosphate buffer solution (pH 7.4) and stirred for 24 h. To confirm the sample expulsion of MXM from the scaffold, the mixture underwent sonication. After filtration, subsequent dilutions were prepared to create standard and working solutions. An established HPLC technique was engaged to examine these solutions and quantify the drug levels. The EE of MXM in each scaffold formulation was calculated using Equation (3), integral to the established analytical procedure. This rigorous process facilitated the assessment of MXM expulsion from the scaffold and provided precise quantification of MXM content using HPLC [25, 26].

$$\% \text{ EE} = \frac{\text{estimated MXM content}}{\text{theoretical MXM content}} \text{X100} \text{ --- (3)}$$

MXM-expulsion from S-MMSs

The *in vitro* expulsion study of MXM from the S-MMSs was conducted using the Franz diffusion cell method. Freshly prepared PBS at pH 7.4 was used at 37 °C. Cellulose acetate membranes with an average pore size of 0.45 µm were pre-soaked in distilled water for 30 min before application to the S-MMS formulation [27, 28].

These membranes were securely placed on top of the receptor chambers within the diffusion cells after filling the chambers with the buffer medium [29]. The donor compartment containing approximately 150 mg of S-MMSs in 10 ml of medium was securely attached to the membrane in the receptor compartment, with stirring at 50 rpm.

At predefined intervals, 0.5 ml samples were withdrawn from the receptor chambers. Following each withdrawal, an equal volume of freshly prepared medium was added back to preserve sink conditions. These samples were appropriately diluted, and the MXM content was quantified using the previously established HPLC.

The scaffolds demonstrating superior EE and Percent Cumulative Drug Released (%CDR) characteristics will be selected for the fabrication of sub-dermal implants.

Preparation of sub-dermal implants

The selected MMSs-loaded scaffolds, each weighing 350 mg and containing 200 mg equivalent MXM, with optimal EE and % CDR (iS-MMS-4, iS-MMS-6, iS-MMS-10, iS-MMS-12, iS-MMS-13, iS-MMS-14, iS-MMS-15, iS-MMS-16, and iS-MMS-17), were included in each formulation. Chitosan was dissolved in 0.1% acetic acid to a concentration of 1-2% w/v and Gelatin in warm water to 2% w/v. Mix these solutions and add Glycerin (1% v/v) to improve flexibility. Combine this mixture with the MXM solution, ensuring thorough homogenization. Pour the resulting mixture into molds or onto a surface to form scaffolds and allow them to set at room temperature or in a controlled environment until solidified. Dry the solidified scaffolds in a drying chamber or oven at 50±2 °C to remove moisture, then sterilize using autoclaving or ethylene oxide gas. Store the sterilized scaffolds in a sterile environment until required. Finally, conduct quality control checks to confirm that the scaffolds meet the necessary standards for consistency, mechanical properties, and biocompatibility. Later, they cut into rod-shaped pieces measuring 6x3 mm [30-32].

Sterilization of implants

The prepared implants underwent sterilization using UV light. They were sited inside a Class II microbiological safety cabinet and exposed to UV light at a wavelength of 360 nm while positioned on a see-saw rocker for 5 min [33].

Statistical assessing

The data were collected and assessed using GraphPad Prism (v. 8.0; San Diego, California, USA), Design Expert version 11 software, and Microsoft Excel 2016. Expressive statistics, including mean±standard deviation, were utilized to summarize the data. Analysis of Variance (ANOVA) was employed to govern variances amid sets, with a significance level established at ($P<0.05$) to designate statistically significant variations. This comprehensive statistical analysis was conducted to offer robust insights into the experimental data and to assess the significance of observed trends and differences within the study.

Implants appraisal

The evaluations performed on the implants focused on assessing their safety, efficacy, and performance [34].

***In vitro* expulsion**

Each implant was individually placed in a 10 ml vial containing Phosphate Buffer Solution (PBS) (pH 7.4). The vials were sealed with rubber stoppers to prevent contamination and then incubated in a controlled environment at 37±0.5 °C. To monitor drug release from the implants, the dissolution fluid was regularly replaced at specified intervals with fresh PBS. Each sample of dissolution fluid was diluted with PBS at pH 7.4 and analyzed spectrophotometrically at 360 nm to determine the MXM concentration [35, 36].

Kinetic modeling

Several kinetic models, such as zero order, first order, Higuchi, Hixson-Crowell, and Korsemeyer-Peppas models, were utilized to analyze the drug release kinetics from the implants. These models serve to elucidate different aspects of drug release mechanisms, including diffusion-driven release (Higuchi model), changes in surface area or solubility (Hixson-Crowell model), constant release rate (zero order model), exponential decrease in drug concentration (first order model), and complex release mechanisms (Korsemeyer-Peppas model). By comparing these models with experimental data, the study aimed to characterize the drug release pattern and mechanism, facilitating formulation optimization and the progress of tailored drug delivery systems [37, 38].

Mechanical assets

To ensure the robustness of the proposed implants, their strength and flexibility must be rigorously assessed. Implants that are too rigid are susceptible to breakage during insertion or while in place, highlighting the need for a balanced level of flexibility to withstand such forces. Adequate strength is also essential to maintain mechanical integrity throughout drug release. Durability is critical to prevent issues like implant rupture, which can lead to increased drug release rates and potential side effects. Evaluation involves determining the maximum force required for breakage and assessing the bending angle at the breakpoint for each implant, ensuring they meet performance and safety standards [39, 40].

Uniformity in MXM

In the MXM preparation process, 10 units of implants were triturated, resulting in a blend equivalent to 600 mg, which was then regimented with PBS at pH 7.4. The MXM content in the mixture was subsequently assessed by spectrophotometry at 360 nm using PBS of pH 7.4 as a diluent. This analytical method facilitated precise measurement of the drug concentration in the final formulation, providing valuable insights for quality control and ensuring accurate dosing in drug delivery applications [41, 42].

Degradation studies

The degradation process for dermal implants followed the International Organization for Standardization (ISO)-10993 standard for evaluating medical device biocompatibility. Implants were immersed in PBS solutions at pH 7.4 and 4.0 for 12 w at 37 °C. Weekly, samples were withdrawn and weighed, and the percentage weight loss was calculated using, e. q.4. This approach ensured precise assessment of degradation rates, critical for evaluating the long-term stability and performance of the implants [43-45].

$$\%\text{mass loss} = \frac{\text{mass (after degradation)} - \text{mass (initial)}}{\text{mass (initial)}} \text{X}100 \text{ --- (4)}$$

Sterility testing

The sterility testing of PLA-based materials, subjected to various sterilization methods including γ-radiation, Microwave (MW) radiation, UV light, and non-sterilized controls, followed British Pharmacopoeia standards. Two culture media were used: soya-bean casein digest media for aerobic bacteria and fluid thioglycollate media for anaerobic bacteria, as per protocol requirements. Positive controls with *Staphylococcus aureus* and *Escherichia coli*, and a negative control using sterile PBS at pH 7.4, were included. Incubation temperatures were maintained at 20-25 °C for soya-bean casein digest media and 30-35 °C for fluid thioglycollate media over 14 d. Throughout incubation, samples were regularly monitored for macroscopic signs of microbial growth, such as turbidity [46].

***In vivo* research**

The *in vitro* readings on frequent assessments were managed as per Panezai, *et al.,* 2022 [47]. The authors selected formula-17 (iS-MMS-17) for *in vivo* study as it possesses uniformity in thickness, mechanical strength, MXM content, and other physical assets.

***In vivo* bioavailability assessments**

Krishna Rabbit Farms (Bengaluru) dispatched the New Zealand Wistar rabbits for the *in vivo* study. The study observed the Animal Ethical Guidelines for Laboratory Studies. The institute conducting the study was endorsed by the Committee for Control and Supervision of Experiments on Animals (CCSEA) under approval number 1519/PO/Re/S/11/CCSEA/2023/04. Additionally, the study was sanctioned by the Institutional Animal Ethics Committee (IAEC) with reference number 1582-2.8-018/23 for the execution of animal trials.

This study involved six New Zealand rabbits (both sexes, weighing 2-3 kg each), divided into two groups of three using a parallel design. The objective was to evaluate the pharmacokinetics of the selected implant iS-MMS-17. For adaptation, the rabbits were elated to the animal facility at least one week before the first treatment, housed individually in separate cages at normal room temperature, under a 12/12 h night-day cycle, with free access to food and water, and handled according to current guidelines on animal welfare. The iS-MMS-17 implants (6x3 mm) were washed with sterile Dulbecco's Modified Eagle (DMEM) medium comprising 100 U/ml of penicillin G, 25 µg/ml of gentamicin, and 0.5 µg/ml of fungizone, tailed by a 24 h incubation at 37 °C in DMEM covering antibiotics and fungizone. Before implantation, the implants were treated with sterile 0.9% saline solution for 5 min to eliminate the culture medium. The rabbits were locally anesthetized with lignocaine (0.05 ml/10 g), and the implantation area was organized by splintering and washing twice with povidone and 70% ethanol. A 6x3 mm implant was aseptically introduced subcutaneously, and the incision was closed with 3-4 cutaneous silk and 4/0 stitches. Post-implantation, the rabbits were retained independently and given food and water ad libitum. Group-A rabbits received iS-MMS-17 implants, while Group-B rabbits received pure drug implants (without microspheres and scaffold formulation). Blood samples (0.5 ml) were taken into heparinized tubes at 0, 12, 24, 36, 48, 60, and 72 h post-implantation. Heparinized whole blood and plasma were separated by centrifugation at 3,500 rpm for 15 min. Plasma samples were transferred to Eppendorf tubes and stored at-20 °C until analysis and assessed by HPLC [48, 49].

Approximation of MXM in plasma samples

MXM in the plasma samples were appraised according to the HPLC process [50].

Making of standard plot

The technique was implemented as described by Sun *et al.* in 2023, with a few minor adjustments. For the stock solution, 100 mg of MXM was precisely weighed and relocated to a 100 ml volumetric flask, where it was dissolved using sonication in the Mobile Phase (MP), and the final volume was adjusted with the MP. These stock

solutions were used to create working standard solutions, which contained 10-90 µg of MXM [51].

Making of the impaled plasma sample

The method adopted for this study was described by Kaya *et al.*, 2022 [52]. A mixture of 250 µl** of rabbit plasma, 50 µl** of internal standard, 10 µl** of MXM, and 2 ml of acetonitrile was pipetted into a 10 µl** centrifuge tube. After centrifuging the mixture for 10 min at 3500 rpm, 10 µl** of the supernatant was collected, placed in the HPLC, and a chromatogram was produced [53].

Process development

Freshly prepared buffer, 0.1% acetonitrile, and 0.1% o-phosphoric acid were combined in a 60:40 (v/v) ratio as the MP, which worked very well for separation. Then, flow rates of 0.4, 0.8, 1.0, 1.2, and 1.5 ml/min were tested. A graph was obtained after 10 µl** of the supernatant (isolated after centrifugation at 3500 rpm for 10 min) was fed into the HPLC, which offered a better resolution of the peaks [54].

Finding the pharmacokinetic constraints

The Area Under the Curve (AUC), peak levels (C_{max}), time at which the drug peaks (t_{max}), biological half-life (t½), percentage absorbed at several time points, and elimination rate constant (Kel) were all determined from the time vs. plasma concentrations of MXM data. The C_{max} and the t_{max} were determined by calibration curves. The plasma level and time measurements were plotted on a semi-logarithmic chart. Kel was assessed during the elimination phase using the slope of the linear line. The percentage absorbed at various times and the absorption rate constant (Ka) were determined using the Wagner and Nelson equation [55]. The t½ was calculated as 0.693/Kel. The trapezoidal rule was used to estimate the AUC. The lingering area from 10 h to time was planned by eq. 5 and 6.

$$[AUC]_{8-\infty} = \text{Levels at 10 h}/K_{el} \text{ ---- 5}$$

$$\text{then } [AUC]_{0-\infty} = [AUC]_{0-10}\text{h} + [AUC]_{10-\infty}\text{h} \text{ --- 6}$$

***In vivo* examination procedure**

To compute Animal Equivalent Dose (AED) from Human Dose by eq.7 was used [56].

$$AED = \frac{\text{Human Dose (mg/kg)}}{\text{Animal weight (kg)}} \text{X Human weight (kg)}^{0.33} \text{ --- 7}$$

The equation for calculating the AED was used to project the required dose for the rabbits. Given that a 70 kg human requires 50 mg, the AED for the rabbits was computed as 2.21 mg/kg of MXM [57-59].

Treatment of animals

Six New Zealand rabbits (both sexes, 2-2.25 kg) were divided into two groups of three using a parallel design, with the study approved by the IAEC. The pharmacokinetics of the iS-MMS-17 were examined. The rabbits were acclimatized for at least one week before the first treatment, housed individually with a 12/12-h night-day cycle, normal room temperature, and free entree to food and water, rendering to current animal welfare guidelines. Implants (6x3 mm) were washed in a sterile DMEM medium with penicillin G (100 UI ml^{-1}), gentamicin (25 µg ml^{-1}), and fungizone (0.5 µg ml^{-1}), then incubated for 24 h at 37 °C. Before implantation, the implants were treated with sterile 0.9% saline solution for 5 min to remove the culture medium. The rabbits' local areas were anesthetized with lignocaine (0.05 ml/10g), shaved, and washed twice with povidone and 70% ethanol. A 6x3 mm piece of the implant was introduced subcutaneously and the skin was sutured with 3-4 cutaneous silk and 4-0 stitches. Group-A received MXM microsphere implants, while Group-B received iS-MMS-17 implants. Blood samples (0.5 ml) were collected at 0, 1, 2, 3, 4, 5, 6, and 7 d post-implantation, placed in heparinized tubes, and centrifuged at 3,500 rpm for 15 min. Plasma was separated and stored at-20 °C in Eppendorf tubes until analysis, and MXM plasma levels were determined using HPLC analysis[60-62].

RESULTS

DSC

The DSC thermograms played a crucial role in analyzing the thermal behavior of both pure MXM and MXM within the S-MMSs. Pure MXM exhibited distinct peaks near its melting point (255 °C), indicating a sharp melting profile. Remarkably, the DSC thermogram of the prepared implant displayed peaks at 254.17 °C, closely resembling those of pure MXM. This similarity suggests a uniform distribution of MXM and all formulation components within the implant structure, ensuring homogeneity across the sample. Such uniformity is essential for maintaining consistent drug discharge characteristics and optimizing the overall presentation of the implant system (fig. 1).

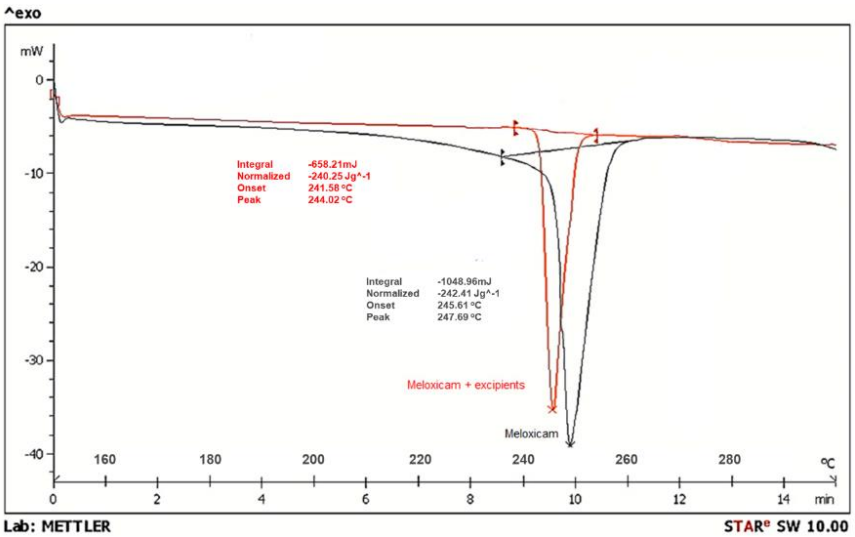

Fig. 1: DSC thermogram of MXM and MXM with excipients

FTIR outcome

FTIR studies were employed to investigate potential interactions between MXM and S-MMSs, providing insights into their chemical functional groups and interactions. The analysis revealed no significant structural interactions, indicating that MXM could be encapsulated within the S-MMSs without compromising the integrity of the formulation components. This supports the suitability of the formulation for effective drug delivery, affirming its potential application in pharmaceutical settings (fig. 2).

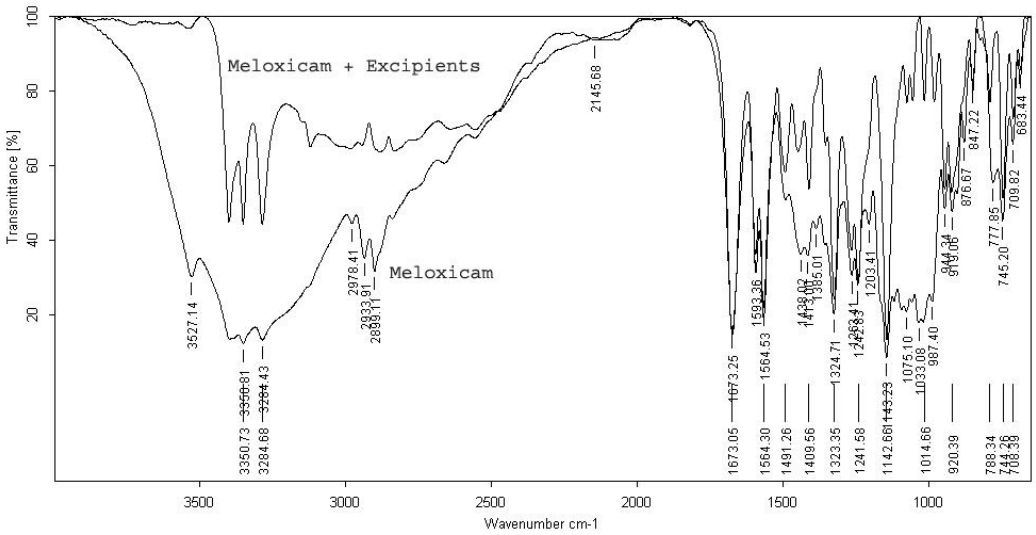

Fig. 2: FTIR spectrum of MXM and MXM with excipients

FTIR spectra of MXM and MXM with excipients

These analytical approaches, including DSC and FTIR, provide valuable insights into the structural and chemical characteristics of the components, interactions between them, and any changes occurring during formulation. The observed phase transitions to amorphous forms and the absence of significant interactions validates the scaffold's suitability as a carrier for drug encapsulation. This reinforces its potential for efficient drug delivery while maintaining desired properties intact.

Evaluation results for microspheres

The results of the MMSs are defined below.

Particle size

The reported PS range of MMS-1 to MMS-9, ranging from 32.5±0.21 to 38.91±0.15 µm, underscores the meticulous precision and quality control maintained throughout their production process. The same procedure was adopted to check the surface morphology (fig. 3).

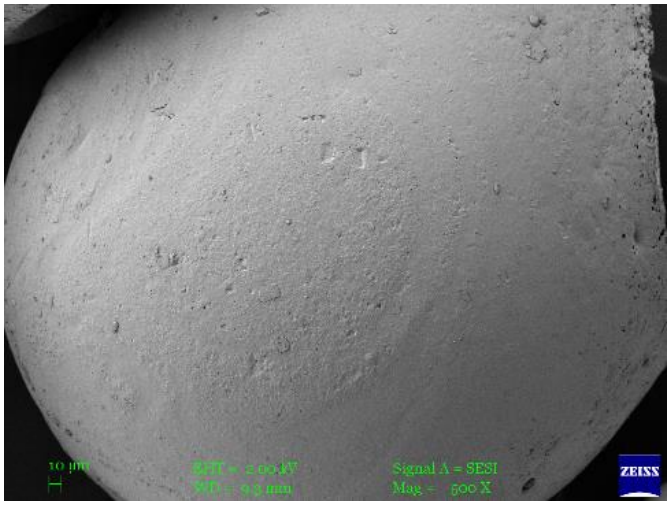

Fig. 3: SEM view showing the surface morphology of microspheres

The yield

The reported percent yield of MMS-1 to MMS-9 microspheres falls within the range of 81.23±1.46% to 98.64±3.65%. These values represent the efficiency of the production process, signifying the percentage of the expected microspheres that were gained. The reported mucoadhesion time for MMS-1 to MMS-9 microspheres falls within the range of 91.23±3.17 to 99.08±3.65 min (fig. 4).

Evaluation results of scaffolds

Appearance and surface morphology

The SEM analysis revealed an intriguing finding: scaffold structures forming three-dimensional arrays designed to effectively secure and retain administered drug molecules within their matrix. This observation underscores the structural integrity and functionality of the scaffolds for drug delivery applications (fig. 5).

The SEM analysis revealed a significant finding about the scaffold structures, showing intricate three-dimensional arrays designed to securely encapsulate and retain administered drug molecules within their matrix. This discovery highlights the robust structural integrity and functional efficacy of the scaffolds in drug delivery applications. For table 3, it would be beneficial to detail the composition of different S-MMSs optimized by BBD, along with their respective % EE and MXM expulsion data.

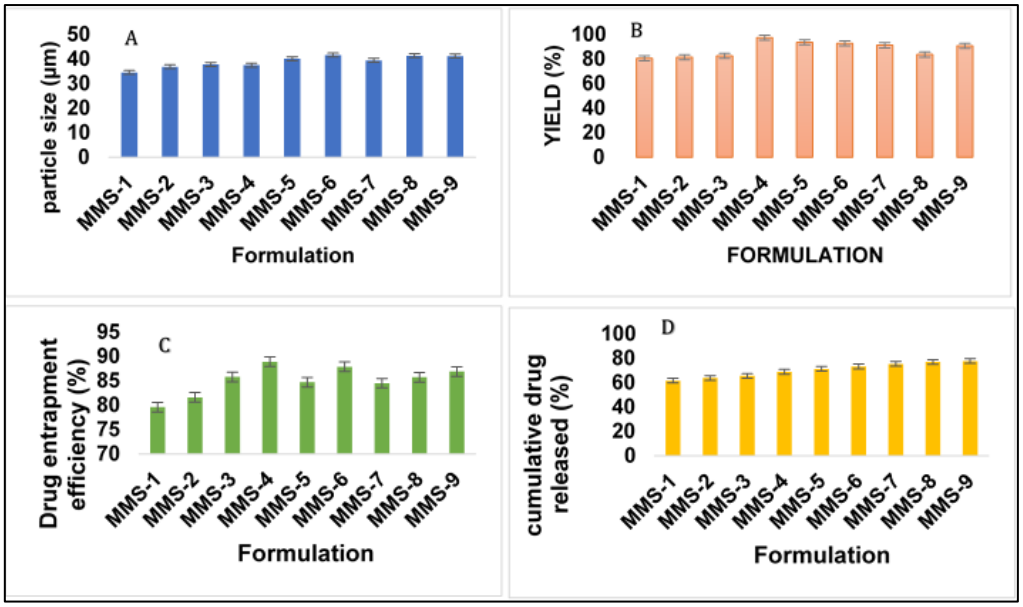

Fig. 4: A) Particle size; B) % yield; C) % entrapment efficiency; D) %MXM expulsion from the microspheres (at 10th h) (values are in mean±SD; n=3)

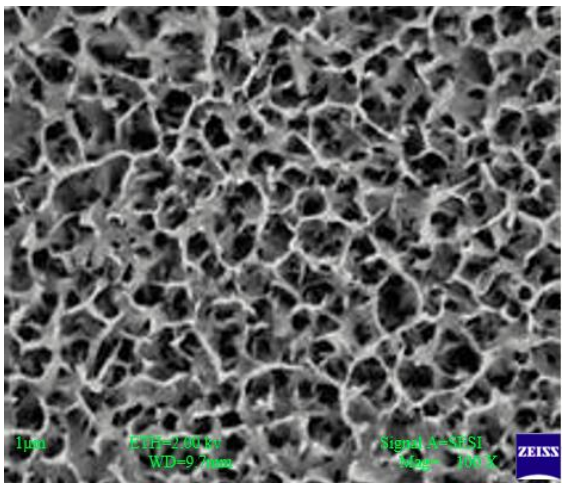

Fig. 5: SEM view displays the surface morphology of MXM scaffolds

Table 3: The response values of the scaffolds

Scaffolds	Response 1 (EE %)	Response 2 (CDR %)
S-MMS-1	61.28±0.28	58.22±1.25
S-MMS-2	62.09±0.35	59.85±0.25
S-MMS-3	63.38±0.14	60.25±0.36
S-MMS-4	64.35±0.11	61.02±0.95
S-MMS-5	67.94±0.08	64.95±0.45
S-MMS-6	71.81±0.07	68.85±0.81
S-MMS-7	73.62±1.06	70.04±0.32
S-MMS-8	75.15±0.25	72.95±0.08
S-MMS-9	79.98±1.36	76.94±0.02
S-MMS-10	83.02±0.45	80.02±0.35
S-MMS-11	85.84±1.24	82.39±0.88
S-MMS-12	85.97±3.54	82.48±0.64
S-MMS-13	86.00±4.26	83.62±0.28
S-MMS-14	86.97±1.25	84.58±0.71
S-MMS-15	87.84±0.65	84.75±0.45
S-MMS-16	88.26±0.45	85.26±0.31
S-MMS-17	89.00±0.75	85.90±0.14

S-MMS: Scaffolds of Meloxicam Microspheres; EE: Entrapment efficiency; CDR: Cumulative Drug Released; values are in mean±SD; (n=3)

Elevated levels of gelatin and plasticizer contribute to increased scaffold integrity and flexibility, consequently enhancing the EE of MXM. Conversely, lower levels of gelatin and plasticizer yield reduced scaffold integrity and flexibility, resulting in slower EE of MXM within the gelatin scaffold. The EE data adhered to a quadratic model, and the software-generated polynomial equations are detailed below:

$$EE=+87.61+0.897A+0.9412B+2.23C+0.04AB-0.585AC-0.7275BC-18.21A^2-6.63B^2+2.72C^2$$

This analysis underscores the intricate relationship between the levels of gelatin and plasticizer, scaffold integrity, and the EE of MXM, highlighting the optimization potential of these factors in controlling the EE of MXM within the scaffold formulations. The constant term,+87.61, is the intercept and signifies the value of EE when all independent variables are set to zero. The coefficients associated with inputs, such as+0.897A,+0.9412B, and+2.23C, designate how EE changes when these variables increase by one unit while holding others constant. Terms like+0.04AB,-0.585AC, and-0.7275BC denote interactions between the independent variables, suggesting how their combined effects influence EE. Lastly, the quadratic terms-$18.21A^2$,-$6.63B^2$, and+$2.72C^2$, reflect the nonlinear influence of each variable individually, demonstrating that the relationship between EE and these variables isn't purely linear. The analysis of variance indicated that all studied formulation factors were statistically significant ($p<0.05$) concerning the EE of MXM within the scaffold, emphasizing the essential role of these factors in determining the EE of MXM.

MXM expulsion

The coded equation for the MXM expulsion can be epitomized as $DR=+84.82+1.15A+0.7962B+2.14C-0.215AB-0.2475AC-0.7475BC-18.12A^2-6.86B^2+2.5C^2$. The constant term,+84.82, represents the intercept, indicating the value of MXM expulsion when all independent variables are zero. The coefficient-1.15A suggests that for each unit increase in A, MXM expulsion decreases by 1.15 units, provided other variables remain unchanged. On the other hand, an increase of 0.7962B results in a significant reduction in MXM expulsion, lowering it by 0.7962 units while keeping other variables constant. An increase of+2.14C, on the other hand, results in an increase in MXM expulsion by 2.14 units, assuming other variables are continuous. The term-0.215AB indicates an interaction effect between A and B, suggesting that their combined influence results in a decrease of 0.215 units in MXM expulsion when both A and B increase by one unit. The term-0.2475AC represents the interaction between A and C, signifying that their combined effect leads to a decrease of 0.2475 units in MXM expulsion when both A and C increase by one unit. The term-0.7475BC represents the interaction between B and C, implying that their combined effect results in a decrease of 0.7475 units in MXM expulsion when both B and C increase by one unit. The quadratic term-$18.12A^2$ signifies that as the value of A increases, MXM expulsion decreases at an accelerating rate. The quadratic term-$6.86B^2$ suggests that as the value of B increases, MXM expulsion decreases at an accelerating rate. The quadratic term+$2.5C^2$ indicates that as the value of C increases, MXM expulsion increases at an accelerating rate (table 4).

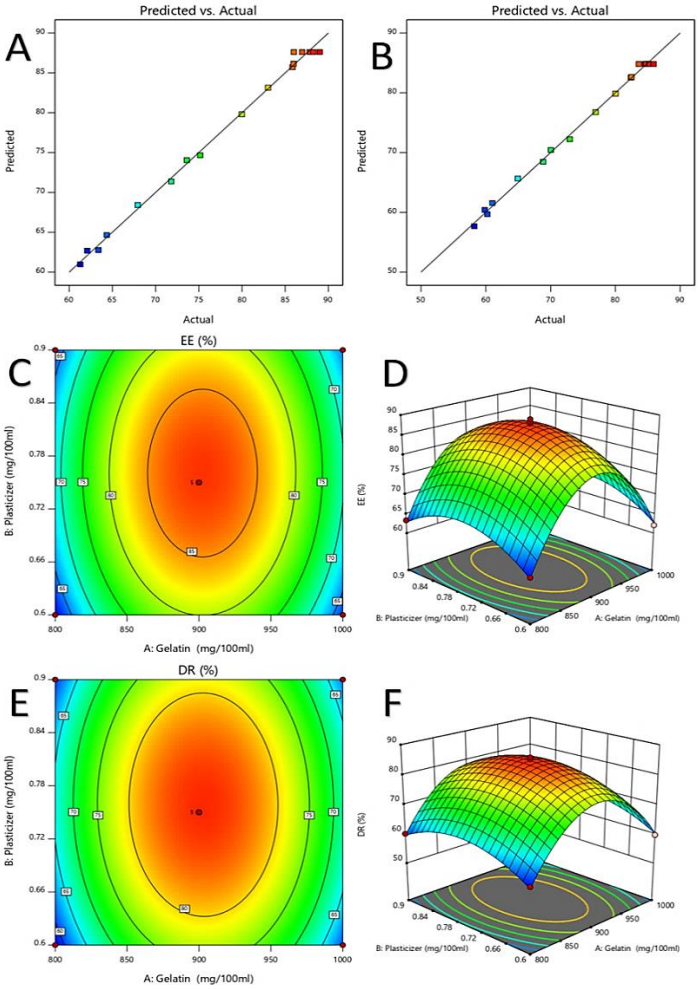

Fig. 6: A) The graphs of predicted versus actual results of the entrapment of MXM; B) predicted versus actual results of the expulsion of MXM from the scaffold; C) contour response surface plot indicating specific interactions and effects on the entrapment efficiency of MXM from the prepared scaffolds; D) 3D response surface plot indicating specific interactions and effects on the EE of MXM from the prepared scaffolds; E) Contour plot indicating specific interactions and effects on the MXM expulsion from the prepared scaffolds; F) 3D response surface plot indicating specific interactions and effects on the MXM expulsion from the prepared scaffolds

Table 4: ANOVA for the quadratic model and studied responses from S-MMSs

FACTORS	MXM Entrapment (Y_1)		MXM expulsion (Y_2)	
	p Value	f Value	*p* Value	f Value
Quadratic model	<0.0001	183.24	<0.0001	240.63
A (Gelatin level)	0.0411	6.24	0.0079	13.50
B (Propylene glycol level)	0.0344	6.86	0.0386	6.46
C (Freezing Time)	0.0004	38.48	0.0002	46.53
AB	0.9395	0.0062	0.6424	0.2354
AC	0.2874	1.33	0.5939	0.3119
BC	0.1953	2.05	0.1355	2.85
A^2	<0.0001	1351.24	<0.0001	1760.69
B^2	<0.0001	179.38	<0.0001	252.52
C^2	0.0009	30.20	0.0007	33.48

The % expulsion of MXM from the scaffold loaded with microparticles ranged from 58.22% to 85.9%. Among the scaffold formulations, S-MMS-17 demonstrated the highest MXM expulsion, reaching up to 85.9%. This substantial expulsion could be attributed to the medium levels of gelatin and plasticizer, as well as the average freezing time employed in this formulation. On the other hand, formulation S-MMS-1 displayed a slower and more limited expulsion of MXM at 58.22%. This restrained expulsion might be attributed to the lower levels of formulation variables utilized in the scaffold's preparation. These observations highlight the considerable influence of formulation variables on MXM expulsion kinetics, revealing the potential for controlled MXM expulsion through strategic adjustments in scaffold composition. The ANOVA results underscore the significant influence ($p<0.05$) of all studied formulation factors on the expulsion of MXM from the microparticle-loaded scaffold, affirming the credibility of the findings and indicating that the observed effects are likely genuine rather than random. To elucidate the cumulative influence of formulation variables on scaffold parameters, 3D graphs were employed, offering a comprehensive visual representation of the intricate interplay between formulation factors and their effects on drug expulsion kinetics. These graphs allow for the visualization of multidimensional data, aiding in the identification of optimal conditions for drug expulsion and uncovering potential synergistic or antagonistic effects between different variables. By enhancing interpretability and communicability, this visual approach provides valuable insights into drug delivery mechanisms, facilitating the optimization of formulations for improved therapeutic outcomes (fig. 6).

The R^2 obtained for the EE of MXM and the expulsion of MXM was 0.9958. This R^2 value was notably close to the adjusted R^2 value (0.9903), confirming the adequacy of the applied model. The ratio of the maximum and minimum values for the studied structured variable was found to be<3, indicating there was no need to alter the version. Furthermore, a p-value of<0.05 confirmed the significance of the quadratic version carried out.

The records for all of the responses under investigation confirmed strong alignment with the quadratic model. The suitability and appropriateness of the quadratic model for these dependent variables were also supported by the signal-to-noise ratio, which was calculated to determine adequate precision. A ratio greater than 4 is generally considered adequate, and in this case, the calculated ratios were 77.21 for Y_1 and 74.24 for Y_2 (table 5). These values further validate the adequacy and robustness of the quadratic model used for the studied responses, affirming its effectiveness in accurately representing the experimental data.

Table 5: The statistics analysis of the checks of the practical model for the responses

Source	EE (Y_1)	MXM expulsion (Y_2)
Standard Deviation	1.02	0.8863
Mean	77.21	74.24
C. V%	1.32	1.19
R^2	0.9958	0.9968
Adjusted R^2	0.9903	0.9926
Predicted R^2	0.9780	0.9727
Adeq. Precision	34.1752	39.9408

To enhance validation and optimize the scaffold formulation, a batch of optimized scaffold formulations was synthesized by implementing the recommended optimal levels of the formulation variables, as provided by the Design Expert software. This step ensures that the experimentally validated model and the derived optimal conditions are applied practically, resulting in scaffold formulations with the desired characteristics.

As the scaffolds (S-MMS-9 to S-MMS-17) revealed noticeable EE and %CDR were additionally made into implants.

Results of implant assessment

***In vitro* expulsion studies**

In the study, the expulsion of MXM in a PBS with a pH of 7.4 showed that 65.39% of the MXM was expelled within 6 d. This finding suggests a controlled and gradual expulsion profile of MXM from the formulation over the specified timeframe. Such results are crucial for understanding the drug's expulsion kinetics and can inform the expansion of dosage forms with optimized expulsion characteristics for therapeutic applications, ensuring worthwhile diminishing of possible adverse possessions.

Kinetics of the drug expulsion

By comparing the expulsion data with other kinetic models, the expulsion kinetics of the formulation were investigated. It was discovered that the best model to describe the expulsion pattern was the Korsemeyer-Peppas model. The fact that the n value was >0.5, indicating non-Fickian diffusion, implies a different expulsion mechanism.

Mechanical properties

The analysis produced results that showed no appreciable differences or significant variances in the breaking force across the various implants that were being assessed. Put another way, the results did not indicate any appreciable variations in the maximal force needed to break each implant. This indicates that the strength and structural integrity of the evaluated implants are comparable or uniform (fig. 7).

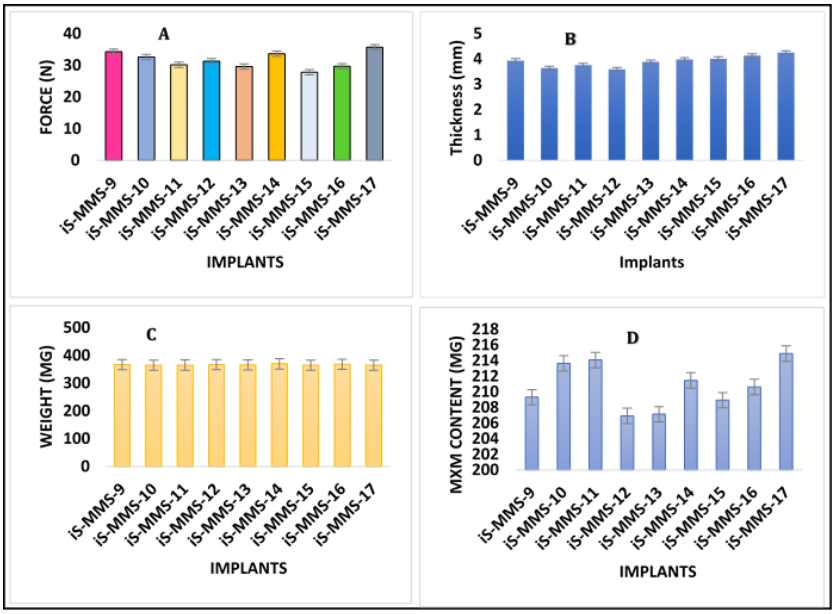

Fig. 7: Physicochemical assets of implants (values are in mean±SD; n=3)

Results of the uniformity in MXM content, thickness, and the weight

The implants established uniformity in thickness (3.45±0.06 to 3.92±0.05 mm), unvarying weight (361.22±3.82 to 369.79±2.95 mg), and even MXM content (206.92±2.56 to 214.08±4.52 mg).

Mass loss in degradation studies

The investigation indicates that the implants demonstrated greater stability when immersed in pH 7.4 PBS compared to pH 4.0 solutions over 100 d. This was evidenced by a significantly higher mass loss observed in the acidic environment (pH 4.0), whereas the implants experienced less mass loss in the neutral environment (pH 7.4). This suggests that the acidic conditions accelerate the degradation process of the implants, while neutral conditions help maintain their integrity for a longer period (fig. 8).

Sterility testing

In the sterilization method employed, no microbial growth was detected in either the soya-bean casein digest medium or the fluid thioglycollate medium throughout the 14 d test period for all the prepared implants, as indicated by the absence of turbidity. It is noteworthy that the negative controls, which comprised an inoculum of the relevant broth with sterile PBS at pH 7.4, also remained devoid of microorganisms throughout the entire fourteen-day experiment, as evidenced by the absence of turbidity. In contrast, the non-sterilized materials and positive controls of *E. coli* and *S. aureus* exhibited microbial growth, as apparent by the existence of turbidity in each case (table 6).

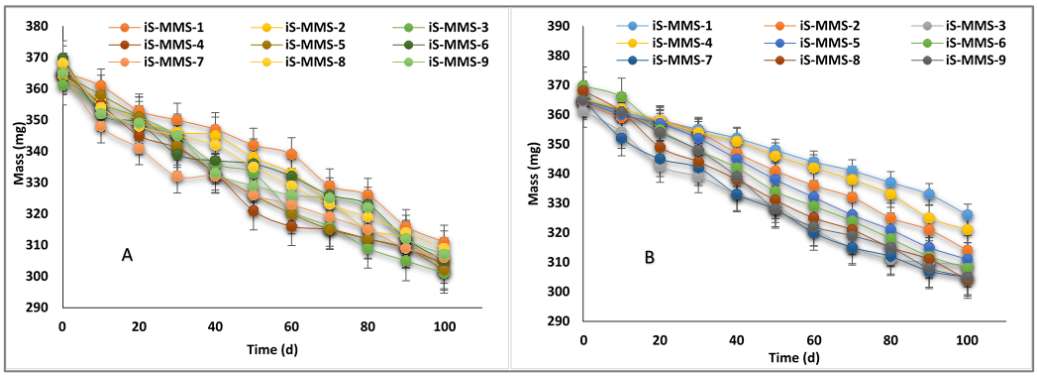

Fig. 8: Trial consequences of diminish in the weight of implants till 100 d in A) pH=4; B) pH=7.4 (values are in mean±SD; n=3)

Table 6: The outcome of the sterility test

Test	Soya bean casein medium	Fluid thioglycollate medium
Negative control	No growth	No growth
E. coli	Microbial growth seen	Microbial growth seen
S. aureus	Microbial growth seen	Microbial growth seen
γ-irradiation	No growth	No growth
Non-sterile	Microbial growth seen	Microbial growth seen

The negative control showed a clear and unclouded appearance, indicating the absence of microbial growth. Positive controls with *E. coli* and *S. aureus* exhibited turbidity, signifying microbial growth. For γ-radiation sterilized samples, a clear appearance

analogous to the negative control would be expected, confirming the efficacy of the sterilization process in preventing microbial contamination. Non-sterilized samples, on the other hand, would likely display turbidity, similar to the positive controls, signifying microbial growth in the absence of sterilization. The sample size was (n=3).

***In vivo* results**

The presence of MXM in the plasma sample is clearly shown by a single, recognizable peak in the HPLC data at 4 min after sample injection. Each plasma sample was taken on days 1 to 7 (fig. 9 and 10). The graphs did not show any noise peaks that may indicate that the medication is present in the plasma.

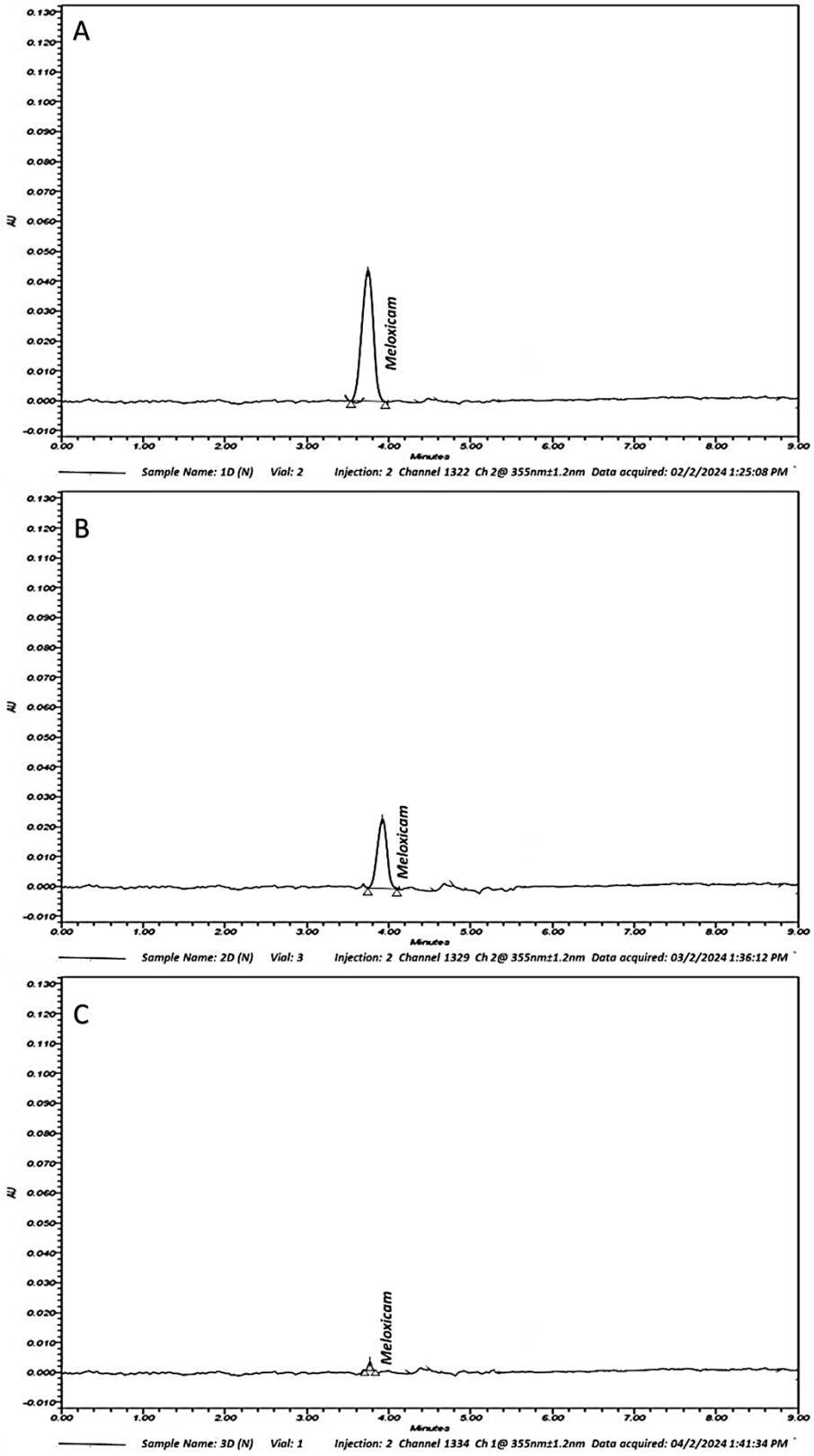

Fig. 9: The graph of the plasma sample with MXM microsphere implants indicating MXM availability in the blood plasma only for 2 d

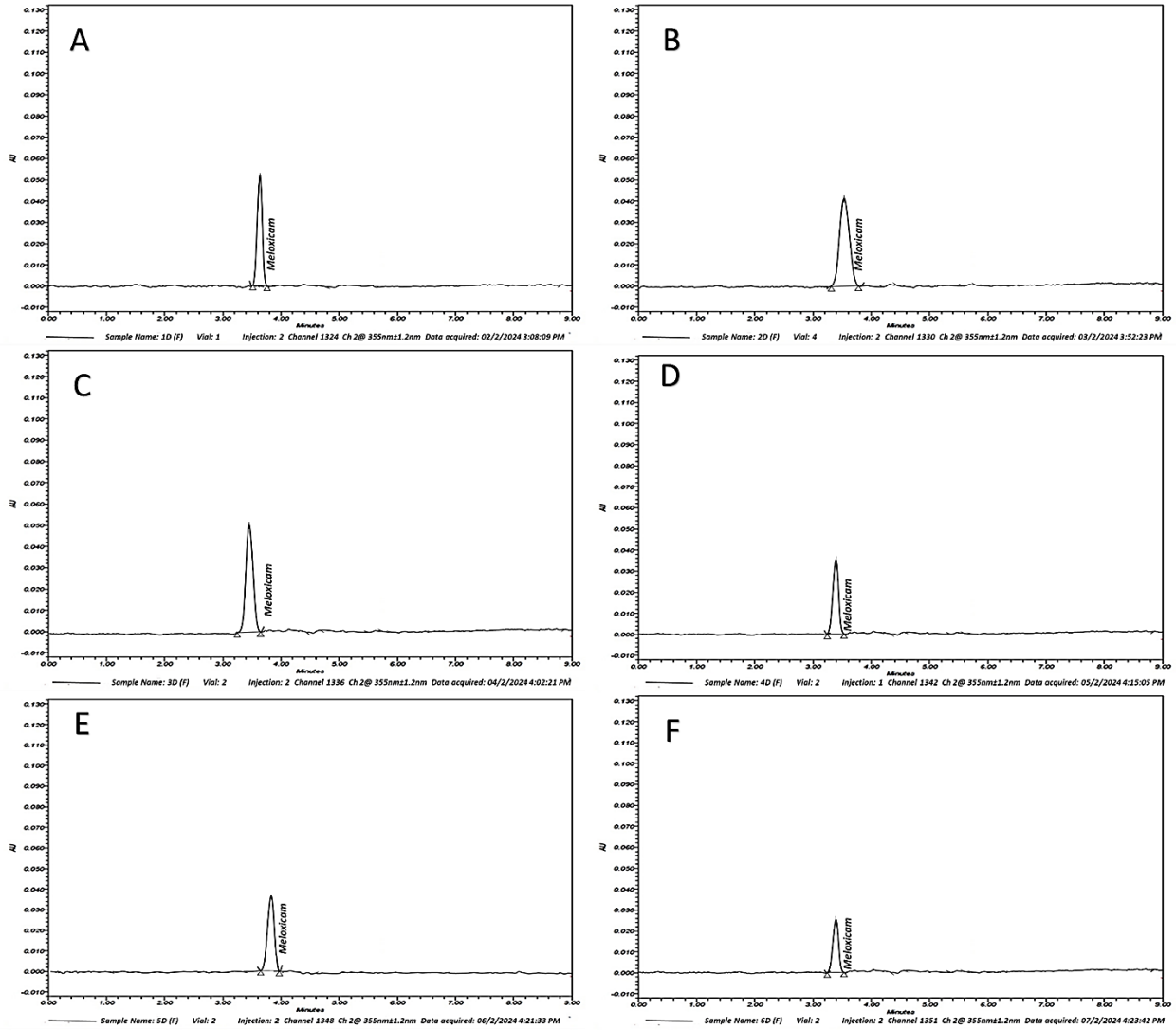

Fig. 10: The graph of the plasma sample with iS-MMS-17 implants indicating its availability in the blood plasma on A) after day 1; B) after day 2; C) after day 3; D) after day 4; E) after day 5; F) after day 6

The retention times from the graphs were 3.81 min on day 1, 3.79 min on day 2, and 3.59 min on day 3. On days 4, 5, and 6, the retention times were 3.44 min, 3.91 min, and 3.43 min, respectively. The peak values reached a maximum of 59,858 on day 1, followed by 39,647 on day 3. The asymmetric factor was highest at 1.52 on day 1 and lowest at 0.62. The arithmetical data of the HPLC graphs indicated linearity between 2-20 µg/ml, with the Limit of Detection (LOD) being highest on day 2 at 0.59 µg/ml and the Limit of Quantification (LOQ) at 1.55 µg/ml. The correlation coefficient was observed to be linear, and other values were found to be significant.

Rabbits were adopted for performing the *in vivo* assessment among various implants, including iS-MMS-4, iS-MMS-6, iS-MMS-10, iS-MMS-12, iS-MMS-13, iS-MMS-14, iS-MMS-15, iS-MMS-16, and iS-MMS-17. iS-MMS-17 was elected due to its promising *in vitro* results.

A single dose of the iS-MMS-17 formulation (MXM: 2.21 mg/kg) showed symmetrical mean C_{max} values (78.88±0.62 µg/ml) greater than those of pure MXM polymer blend implants, indicating the suitability of iS-MMS-17 in the animal model. The T_{max} values for iS-MMS-17 were found to be 8 h, indicating the time at which MXM reached maximum plasma levels. The $AUC_{(0\text{-}10h)}$ was 501.7±5.88 µg. h/ml, and the $AUC_{(0\text{-}\infty)}$ was 648.4±6.84 µg. h/ml, showing the MXM's reachability in the systemic circulation. The Area Under the Moment Curve (AUMC) value for the iS-MMS-17 sample was established to be 483.25±7.21 µg. h^2/ml. The mean residence time in plasma was observed as 13 h, and the t½ was noted as 7.6±0.1 h (fig. 11). All these values were statistically significant, with a P-value<0.05.

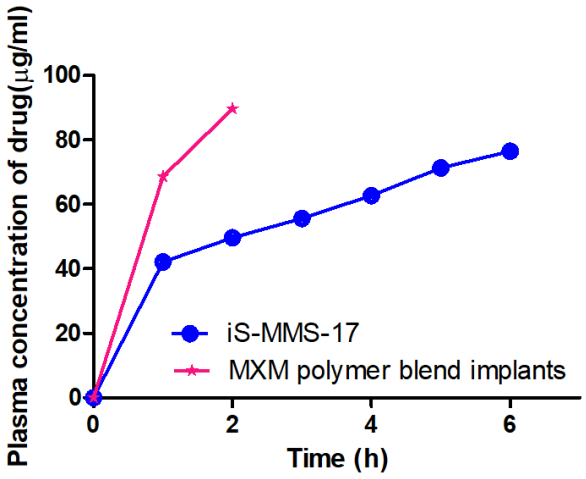

Fig. 11: Mean plasma levels of iS-MMS-17 vs. MXM polymer blend implant (n=3)

DISCUSSION

The DSC analysis confirmed the sharp melting behavior of MXM and revealed a homogeneous distribution of all formulation components within the implant structure. FTIR analysis suggests that MXM and S-MMSs can coexist harmoniously within the formulation, enhancing its potential as an effective drug delivery system. The versatility of MMSs in offering a customizable PS range is pivotal for tailoring drug delivery systems to specific therapeutic needs, from rapid expulsion to targeted delivery.

Overall, the precise control over PS not only ensures quality and efficacy but also drives innovation and advancement in pharmaceutical formulations. Uniform PS in microspheres is paramount as it signifies even distribution of drug molecules within them [63]. Achieving uniform PS is crucial in maximizing therapeutic efficacy and ensuring safety in controlled-expulsion drug delivery systems, as it minimizes side effects associated with erratic drug expulsion, making it a focal point in pharmaceutical progress.

SEM analysis revealed intricately designed scaffold structures forming three-dimensional arrays, proficiently securing and retaining drug molecules within their matrix. This underscores their potential as highly effective drug delivery systems, highlighting the importance of structural engineering in optimizing drug delivery platforms and paving the way for enhanced therapeutic outcomes. The encapsulation of MXM within the S-MMSs suggests that higher concentrations of gelatin and plasticizer positively influence the EE of MXM, up to a certain limit [64].

The scaffold pattern significantly influences EE and %CDR, as variations in gelatin and plasticizer levels contribute to the structural integrity of the gelatin scaffold, influencing EE and expulsion kinetics. Akhila *et al.* (2023) [65] made gelatin scaffolds and observed their drug expulsion. The expulsion percentage of MXM from the scaffold loaded with microparticles varied significantly, ranging from 42.2% to 83%. Notably, S-MMS-17 exhibited the highest expulsion rate at 83%, attributed to lower levels of gelatin and plasticizer, along with a shorter freezing time. Elevated levels of gelatin and plasticizer extended sustained MXM expulsion, but only up to a threshold, with denser scaffold structures limiting expulsion-conversely, lower levels compromised scaffold integrity, resulting in higher expulsion rates. Wu *et al.* (2010) made gelatin scaffolds and found the highest drug expulsion with gelatin scaffolds made with the aid of freeze drying [66].

The expulsion of MXM from the MXM-embedded scaffolds enclosed in subcutaneous implants in a PBS with a pH of 7.4 demonstrated that 65.39% of the drug was expelled within 6 d, indicating a controlled and gradual expulsion profile. This finding provides valuable insight into the drug's expulsion kinetics and informs the progress of dosage forms with optimized expulsion characteristics for therapeutic applications. By understanding the expulsion profile, researchers can tailor formulations to ensure efficacy while suppressing potential adverse effects and enhancing patient outcomes. Abpeikar *et al.* made macroporous scaffolds of MXM using gelatin nanofibers and observed the stability for a week [67].

Understanding how pharmaceutical formulations expel their contents is essential to comprehending how medication delivery systems function. Because it can accurately describe MXM expulsion from polymeric systems (hydrogels, nanoparticles, and matrices), the Korsemeyer-Peppas model is frequently utilized. Because of its adaptability to various expulsion mechanisms, such as diffusion-controlled, swelling-controlled, and erosion-controlled expulsion, it is especially preferred. This study's observation that the value of 'n' in the Korsemeyer-Peppas model is greater than 0.5 denotes non-Fickian diffusion [68].

Optimization of medication distribution and formulation design is significantly influenced by the discovery of non-Fickian diffusion in the expulsion mechanism. It implies that various elements, including polymer properties, formulation composition, and environmental circumstances, influence the expulsion behavior in addition to simple diffusion processes. This study's detection of non-Fickian diffusion emphasizes the intricacy of drug expulsion processes and stresses the significance of taking a variety of aspects into account when designing and optimizing formulations [69].

Uniaxial loading tests conducted at two stages (0 d and 100 d) during degradation showed no significant differences in tensile strength across formulations [70]. The uniformity of implants across parameters such as thickness, weight, and drug content is crucial for ensuring consistent drug delivery and efficacy. Uniform thickness is essential as it determines the surface area available for drug expulsion. A consistent thickness ensures that the rate of drug expulsion remains constant, preventing variability in dosage delivery. Deviations in thickness could lead to uneven drug distribution and subsequently affect the expulsion kinetics of the implant.

Uniform weight is important for dosing accuracy and patient safety. Consistency in weight ensures that each implant contains the intended amount of MXM, suppressing the risk of under- or overdosing. This uniformity is especially critical in controlled expulsion systems where precise drug concentrations are required to maintain therapeutic efficacy over an extended period. Lastly, uniformity in MXM content directly influences the drug's pharmacological effect. Variations in drug content among implants could result in inconsistent therapeutic outcomes, compromising patient treatment. Ensuring uniform MXM content guarantees reliable and predictable drug expulsion, enhancing the reproducibility and effectiveness of the implant. Gobin *et al.* (2006) tested the mechanical assets of silk fibroin and chitosan mixture scaffolds and observed uniformity in the physical constraints [71].

In this investigation, implants displayed greater stability in pH 7.4 buffer solutions compared to pH 4.0 over 100 d, with a notably higher mass loss in acidic environments (14.4% vs. 9.66%). This highlights pH's significant role in accelerating degradation, which is crucial for understanding biomaterial stability and optimizing designs for biomedical use [72-74]. The employed γ-radiation method demonstrated effectiveness in preventing microbial contamination. In contrast, non-sterilized materials and positive controls of *E. coli* and *S. aureus* displayed microbial growth. The clear appearance of the negative control, akin to the expected outcome for γ-radiation-sterilized samples, further validates the efficacy of the sterilization process [75-77].

The *in vivo* study demonstrated that MXM was consistently detectable in plasma samples over seven days, with clear, distinct peaks in HPLC data, confirming its presence without noise interference. Retention times varied slightly, and peak values were highest on day 1, with significant linearity observed in the HPLC analysis. For the *in vivo* assessment, rabbits were used to evaluate various implants, with iS-MMS-17 selected for its superior *in vitro* performance. A single dose of iS-MMS-17 (2.21 mg/kg) showed higher mean C_{max} values (78.88±0.62 µg/ml) than pure MXM polymer blends, with a T_{max} of 8 h and significant AUC values ($AUC_{(0-10h)}$: 501.7±5.88 µg. h/ml, $AUC_{(0-\infty)}$: 648.4±6.84 µg. h/ml). The AUMC was 483.25±7.21 µg. h^2/ml, with a mean plasma residence time of 13 h and a t ½ of 7.6±0.1 h, all statistically significant ($P<0.05$), indicating iS-MMS-17's potential for effective therapy [78, 79].

CONCLUSION

The development of MXM-loaded gelatin microspheres integrated into gelatin scaffolds has shown significant promise as an innovative drug delivery system. This system was designed to enhance drug delivery efficiency and sustain drug release, addressing the crucial need for extended pain relief without adverse effects, ultimately aiming to improve patient outcomes and quality of life. The optimized scaffolds demonstrated robust physicochemical properties, with the microspheres formulated using a 1:1 ratio of PLA and PLGA. These microspheres exhibited favorable characteristics such as smaller PS, high yield, and efficient EE and release. The use of Design Expert software and the BBD method resulted in highly desirable scaffolds, evidenced by a desirability factor close to one across all assessed variables. Sustained drug release over an extended period was achieved, highlighting the potential of these scaffolds for diverse biomedical applications. The implants made from these scaffolds showed greater stability in pH

7.4 PBS compared to pH 4.0 over 100 d, with a higher mass loss observed in acidic environments (14.4% vs. 9.66%). This finding underscores the importance of pH in the degradation of biomaterials and the necessity of optimizing these systems for stability in physiological conditions. The effectiveness of γ-radiation sterilization in preventing microbial contamination was confirmed, as the sterilized implants showed no microbial growth compared to non-sterilized materials. In vivo studies in rabbits confirmed the detection of MXM in plasma samples over seven days, with clear HPLC data showing minimal noise interference. The iS-MMS-17 formulation, selected for its superior *in vitro* performance, demonstrated higher mean C_{max} values (78.88±0.62 µg/ml) compared to pure MXM polymer blends, with a T_{max} of 8 h and significant AUC values ($AUC_{(0\text{-}10h)}$: 501.7±5.88 µg. h/ml, $AUC_{(0\text{-}\infty)}$: 648.4±6.84 µg. h/ml). Additionally, the AUMC was 483.25±7.21 µg. h^2/ml, with a mean plasma residence time of 13 h and a t½ of 7.6±0.1 h, all statistically significant ($P<0.05$). These pharmacokinetic parameters suggest that the iS-MMS-17 formulation holds significant potential for effective pain and arthritis therapy. The prolonged and controlled drug release capabilities of this system enhance patient compliance and improve treatment outcomes, making it a valuable asset in modern pharmaceutical development. Overall, this study concludes that the MXM-loaded gelatin microspheres integrated into gelatin scaffolds are suitable for diverse biomedical applications, offering a promising approach to drug delivery that enhances therapeutic efficacy while minimizing side effects.

ACKNOWLEDGMENT

The authors are thankful to the Institutional Animal Ethical Committee for providing animals and assisting in conducting animal experiments.

FUNDING

Nil

AUTHORS CONTRIBUTIONS

All authors have contributed equally

CONFLICT OF INTERESTS

Declared none

REFERENCES

1. Long T, Tan W, Tian X, Tang Z, HU K, GE L. Gelatin/alginate-based microspheres with sphere in capsule structure for spatiotemporal manipulative drug release in gastrointestinal tract. Int J Biol Macromol. 2023 Jan 31;226:485-95. doi: 10.1016/j.ijbiomac.2022.12.040, PMID 36521695.
2. LI J, Shi H, GU S, Liu F, Han EH. A smart anticorrosive coating based on pH-sensitive microspheres fabricated via a facile method for protection of AA2024-T3. Prog Org Coat. 2024 Apr;189:108259. doi: 10.1016/j.porgcoat.2024.108259.
3. Qingyun F, Zhenzhao G, Dongyin B, KE H, Ziyu S, Weihong J. Multi drug delivery and osteogenic performance of β-tricalcium phosphate/alginate composite microspheres. Int J Polym Mater Polym Biomater. 2024;73(13):1126-35. doi: 10.1080/00914037.2023.2250049.
4. Liu Y, Shi J, Guo Y, Xue Z, Han K, Liu S. Regulating hollow structure of CL-20 microspheres using microjet droplet technology to enhance safety and combustion performance. Fuel. 2024 Apr 1;361:130748. doi: 10.1016/j.fuel.2023.130748.
5. Karnam S, Donthi MR, Jindal AB, Paul AT. Recent innovations in topical delivery for management of rheumatoid arthritis: a focus on combination drug delivery. Drug Discov Today. 2024;29(8):104071. doi: 10.1016/j.drudis.2024.104071, PMID 38942070.
6. Arshad R, Hassan D, Sani A, Mustafa G, Rahdar A, Fathi karkan S. Nano-engineered solutions for ibuprofen therapy: unveiling advanced co-delivery strategies and nanoparticle systems. J Drug Deliv Sci Technol. 2024;98:105815. doi: 10.1016/j.jddst.2024.105815.
7. Zid L, Zelenak V, Almasi M, Zelenakova A, Szucsova J, Bednarcik J. Mesoporous silica as a drug delivery system for naproxen: influence of surface functionalization. Molecules. 2020;25(20):4722. doi: 10.3390/molecules25204722, PMID 33076274.
8. Jang JH, Jeong SH, Lee YB. Dosage exploration of meloxicam according to CYP2C9 genetic polymorphisms based on a population pharmacokinetic-pharmacodynamic model. Pharmacotherapy. 2023;43(2):145-57. doi: 10.1002/phar.2762, PMID 36601711.
9. Yang Z, Liu L, Sheng L, Wang H, LI C, Lin X. Design of an injectable sustained release in situ forming depot of meloxicam for pain relief. J Drug Deliv Sci Technol. 2024;93:105460. doi: 10.1016/j.jddst.2024.105460.
10. Gungor H, Corum O, Durna Corum D, Kumru AS, Yilmaz G, Coskun D. Pharmacokinetics of meloxicam following intravenous administration at different doses in sheep. J Vet Pharmacol Ther. 2024;47(3):202-7. doi: 10.1111/jvp.13422, PMID 38033195.
11. Sharma G, Sharma P, Alam MA. Scaffold-based microsphere in drug delivery system. Int J Nanomater Nanotechnol Nanomed. 2023;10:16-22.
12. Han N, Fang H, Niu R. Nanosphere and microsphere-based drug delivery systems for wound healing applications: a review. Sci Adv Mater. 2023;15(4):441-56. doi: 10.1166/sam.2023.4446.
13. Luo X, Zhang L, Luo Y, Cai Z, Zeng H, Wang T. Charge-driven self-assembled microspheres hydrogel scaffolds for combined drug delivery and photothermal therapy of diabetic wounds. Adv Funct Materials. 2023;33(26):2214036. doi: 10.1002/adfm.202214036.
14. Ruan L, SU M, Qin X, Ruan Q, Lang W, WU M. Progress in the application of sustained release drug microspheres in tissue engineering. Materials Today Bio 2022 Aug 13;16:100394. doi: 10.1016/j.mtbio.2022.100394.
15. Song W, Tong T, XU J, WU N, Ren L, LI M. Preparation and application of green chitosan/ploy (vinyl alcohol) porous microspheres for the removal of hexavalent chromium. Mater Sci Eng B. 2022 Oct;284:115922. doi: 10.1016/j.mseb.2022.115922.
16. Mundarinti SH, Ahad HA. Impact of pistacia lentiscus plant gum on particle size and swelling index in central composite designed amoxycillin trihydrate mucoadhesive microspheres. Ind J Pharm Edu Res. 2023;57(3):763-72. doi: 10.5530/ijper.57.3.93.
17. Babu GN, Muthukaruppan M, Ahad HA. Impact of azadirachta indica fruit mucilage on particle size and swelling index in central composite designed acyclovir mucoadhesive microspheres. Baghdad Sci J. 2023;20(2):425. doi: 10.21123/bsj.2022.6786.
18. Harsha SS, Ahad HA, Haranath C, Dasari RR, Gowthami M, Varam NJ. Exfoliation technique of composing and depictions of clopidogrel bisulphate afloat microspheres. J Evol Med Dent Sci. 2020;9(14):1156-60. doi: 10.14260/jemds/2020/251.
19. Singh S, Devi A, Sharma S, Sabharwal S, Sharma S, Dhiman S. A review on microspheres and its role in different drug delivery system as a novel approach. Int J Pharm Sci. 2024;2(6):1112-26.
20. LI Z, Feng X, Luo S, Ding Y, Zhang Z, Shang Y. High drug loading hydrophobic cross-linked dextran microspheres as novel drug delivery systems for the treatment of osteoarthritis. Asian J Pharm Sci. 2023;18(4):100830. doi: 10.1016/j.ajps.2023.100830, PMID 37588991.
21. Reddy PL, Shanmugasundaram S. Optimizing process parameters for controlled drug delivery: a quality by design (QBD) approach in naltrexone microspheres. AAPS Pharm Sci Tech. 2024;25(5):105. doi: 10.1208/s12249-024-02830-w, PMID 38724807.
22. P LR, Shanmugasundaram S. QBD approach for design and characterization of pramlintide microspheres for controlled drug release. J Pharm Innov. 2023;18(4):2325-47. doi: 10.1007/s12247-023-09795-6.
23. Siraskar PR, Mishra DK. *In vivo* estimation of optimized floating microspheres design by QBD approach. Res J Pharm Technol. 2023;16(8):3697-700. doi: 10.52711/0974-360X.2023.00608.
24. Asha BR, Goudanavar P, Koteswara Rao GS, Gandla K, Raghavendra Naveen N, Majeed S. QBD driven targeted pulmonary delivery of dexamethasone loaded chitosan

microspheres: biodistribution and pharmacokinetic study. Saudi Pharm J. 2023;31(9):101711. doi: 10.1016/j.jsps.2023.101711, PMID 37564747.
25. Karmakar S, Poddar S, Khanam J. Understanding the effects of associated factors in the development of microsponge based drug delivery: a statistical quality by design (QBD) approach towards optimization. AAPS Pharm Sci Tech. 2022;23(7):256. doi: 10.1208/s12249-022-02409-3, PMID 36114372.
26. Alnaim AS, Shah H, Nair AB, Mewada V, Patel S, Jacob S. QBD based approach to optimize niosomal gel of levosulpiride for transdermal drug delivery. Gels. 2023;9(3):213. doi: 10.3390/gels9030213, PMID 36975662.
27. Elkady OA, Tadros MI, El Laithy HM. QBD approach for novel crosslinker free ionotropic gelation of risedronate sodium chitosan nebulizable microspheres: optimization and characterization. AAPS Pharm Sci Tech. 2019;21(1):14. doi: 10.1208/s12249-019-1561-2, PMID 31807950.
28. Patil K, Gujarathi N, Sharma C, Ojha S, Goyal S, Agrawal Y. Quality by design-driven nanostructured lipid scaffold of apixaban: optimization characterization and pharmacokinetic evaluation. Pharmaceutics. 2024;16(7):910. doi: 10.3390/pharmaceutics16070910, PMID 39065607.
29. Munot NM, Shinde YD, Shah P, Patil A, Patil SB, Bhinge SD. Formulation and evaluation of chitosan PLGA biocomposite scaffolds incorporated with quercetin liposomes made by QBD approach for improved healing of oral lesions. AAPS Pharm Sci Tech. 2023;24(6):147. doi: 10.1208/s12249-023-02584-x, PMID 37380851.
30. Farazin A, Mahjoubi S. Dual functional hydroxyapatite scaffolds for bone regeneration and precision drug delivery. J Mech Behav Biomed Mater. 2024 Sep;157:106661. doi: 10.1016/j.jmbbm.2024.106661, PMID 39018918.
31. Zielinska A, Karczewski J, Eder P, Kolanowski T, Szalata M, Wielgus K. Scaffolds for drug delivery and tissue engineering: the role of genetics. J Control Release. 2023 Jul;359:207-23. doi: 10.1016/j.jconrel.2023.05.042, PMID 37286137.
32. Magill E, Demartis S, Gavini E, Permana AD, Thakur RR, Adrianto MF. Solid implantable devices for sustained drug delivery. Adv Drug Deliv Rev. 2023 Aug;199:114950. doi: 10.1016/j.addr.2023.114950, PMID 37295560.
33. Muhindo D, Ashour EA, Almutairi M, Repka MA. Development of subdermal implants using direct powder extrusion 3D printing and hot-melt extrusion technologies. AAPS Pharm Sci Tech. 2023;24(8):215. doi: 10.1208/s12249-023-02669-7, PMID 37857937.
34. Al Litani K, Ali T, Robles Martinez PR, Buanz A. 3D printed implantable drug delivery devices for womens health: formulation challenges and regulatory perspective. Adv Drug Deliv Rev. 2023 Jul;198:114859. doi: 10.1016/j.addr.2023.114859, PMID 37149039.
35. Gunawardana M, Remedios Chan M, Sanchez D, Fanter R, Webster S, Webster P. Preclinical considerations for long-acting delivery of tenofovir alafenamide from subdermal implants for HIV pre-exposure prophylaxis. Pharm Res. 2023;40(7):1657-72. doi: 10.1007/s11095-022-03440-6, PMID 36418671.
36. Behrends W, Wulf K, Raggl S, Frohlich M, Eickner T, Dohr D. Dual drug delivery in cochlear implants: *in vivo* study of dexamethasone combined with diclofenac or immunophilin inhibitor MM284 in guinea pigs. Pharmaceutics. 2023;15(3):726. doi: 10.3390/pharmaceutics15030726, PMID 36986587.
37. Jarosz M, Pawlik A, Szuwarzynski M, Jaskula M, Sulka GD. Nanoporous anodic titanium dioxide layers as potential drug delivery systems: drug release kinetics and mechanism. Colloids Surf B Biointerfaces. 2016;143:447-54. doi: 10.1016/j.colsurfb.2016.03.073, PMID 27037782.
38. Wojcik Pastuszka D, Krzak J, Macikowski B, Berkowski R, Osinski B, Musial W. Evaluation of the release kinetics of a pharmacologically active substance from model intra articular implants replacing the cruciate ligaments of the knee. Materials (Basel). 2019;12(8):1202. doi: 10.3390/ma12081202, PMID 31013801.
39. Suh MS, Kastellorizios M, Tipnis N, Zou Y, Wang Y, Choi S. Effect of implant formation on drug release kinetics of in situ forming implants. Int J Pharm. 2021;592:120105. doi: 10.1016/j.ijpharm.2020.120105, PMID 33232755.
40. Zamoume O, Thibault S, Regnie G, Mecherri MO, Fiallo M, Sharrock P. Macroporous calcium phosphate ceramic implants for sustained drug delivery. Mater Sci Eng C. 2011;31(7):1352-6. doi: 10.1016/j.msec.2011.04.020.
41. Kunrath MF, Shah FA, Dahlin C. Bench to bedside: feasibility of nano-engineered and drug delivery biomaterials for bone-anchored implants and periodontal applications. Materials Today Bio. 2023 Feb;18:100540. doi: 10.1016/j.mtbio.2023.100540.
42. Alshimaysawee S, Fadhel Obaid R, Al Gazally ME, Alexis Ramirez Coronel A, Bathaei MS. Recent advancements in metallic drug eluting implants. Pharmaceutics. 2023;15(1):223. doi: 10.3390/pharmaceutics15010223, PMID 36678852.
43. Zlomke C, Barth M, Mader K. Polymer degradation induced drug precipitation in PLGA implants why less is sometimes more. Eur J Pharm Biopharm. 2019;139:142-52. doi: 10.1016/j.ejpb.2019.03.016, PMID 30902733.
44. Singh M, Gill AS, Deol PK, Agrawal A, Sidhu SS. Drug-eluting titanium implants for localised drug delivery. J Mater Res. 2022;37(16):2491-511. doi: 10.1557/s43578-022-00609-y.
45. Lehner E, Liebau A, Menzel M, Schmelzer CE, Knolle W, Scheffler J. Characterization of PLGA versus peg-plga intracochlear drug delivery implants: degradation kinetics morphological changes and pH alterations. J Drug Deliv Sci Technol. 2024 Sep;99:105972. doi: 10.1016/j.jddst.2024.105972.
46. Chavda VP, Jogi G, Paiva Santos AC, Kaushik A. Biodegradable and removable implants for controlled drug delivery and release application. Expert Opin Drug Deliv. 2022;19(10):1177-81. doi: 10.1080/17425247.2022.2110065, PMID 35929995.
47. Panezai J, Van Dyke T. Polyunsaturated fatty acids and their immunomodulatory actions in periodontal disease. Nutrients. 2023;15(4):821. doi: 10.3390/nu15040821, PMID 36839179.
48. Matusiewicz H. Potential release of *in vivo* trace metals from metallic medical implants in the human body: from ions to nanoparticles a systematic analytical review. Acta Biomater. 2014;10(6):2379-403. doi: 10.1016/j.actbio.2014.02.027, PMID 24565531.
49. Wang X, Burgess DJ. Drug release from in situ forming implants and advances in release testing. Adv Drug Deliv Rev. 2021;178:113912. doi: 10.1016/j.addr.2021.113912, PMID 34363860.
50. Wang X, Roy M, Wang R, Kwok O, Wang Y, Wang Y. Towards *in vitro in vivo* correlation models for in situ forming drug implants. J Control Release. 2024 Aug;372:648-60. doi: 10.1016/j.jconrel.2024.06.058, PMID 38936743.
51. Sun Z, LI M, Qian S, GU Y, Huang J, LI J. Development of a detection method for 10 non-steroidal anti-inflammatory drugs residues in four swine tissues by ultra-performance liquid chromatography with tandem mass spectrometry. J Chromatogr B Analyt Technol Biomed Life Sci. 2023 May 15;1223:123722. doi: 10.1016/j.jchromb.2023.123722, PMID 37099884.
52. Kaya DI, Satır S, Oztas B, Yıldırım H. Avoiding sinus floor elevation by placing a palatally angled implant: a morphological study using cross-sectional analysis determined by CBCT. Diagnostics (Basel). 2024;14(12):1242. doi: 10.3390/diagnostics14121242, PMID 38928657.
53. Onder YB, Alpaslan NZ. Peri-implant phenotype calprotectin and MMP-8 levels in cases diagnosed with peri-implant disease. Clin Oral Investig. 2024;28(7):404. doi: 10.1007/s00784-024-05798-w, PMID 38940878.
54. Yuksel M, Kaya SN. Speech perception as a function of the number of channels and channel interaction in cochlear implant simulation. Medeni Med J. 2023;38(4):276-83. doi: 10.4274/MMJ.galenos.2023.73454, PMID 38148725.
55. Gohel M, Delvadia R, Parikh D, Zinzuwadia M, Soni C, Sarvaiya K. Simplified mathematical approach for back calculation in wagner nelson method: applications in *in vitro* and *in vivo* correlation (IVIVC) and formulation development work. Pharm Rev. 2005;3:1-8.
56. Xiong J, XU Y, HE S, Zhang Y, Wang Z, Wang S. Pharmacokinetics and bioavailability of tildipirosin in rabbits following single-dose intravenous and intramuscular administration. J Vet Pharmacol Ther. 2020;43(5):448-53. doi: 10.1111/jvp.12882, PMID 32542744.

57. Nair AB, Jacob S. A simple practice guide for dose conversion between animals and human. J Basic Clin Pharm. 2016;7(2):27-31. doi: 10.4103/0976-0105.177703, PMID 27057123.
58. Jacob S, Nair AB, Morsy MA. Dose conversion between animals and humans: a practical solution. Indian J Pharm Educ Res. 2022;56(3):600-7. doi: 10.5530/ijper.56.3.108.
59. Nair A, Morsy MA, Jacob S. Dose translation between laboratory animals and human in preclinical and clinical phases of drug development. Drug Dev Res. 2018;79(8):373-82. doi: 10.1002/ddr.21461, PMID 30343496.
60. Elmeliegy M, Udata C, Liao K, Yin D. Considerations on the calculation of the human equivalent dose from toxicology studies for biologic anticancer agents. Clin Pharmacokinet. 2021;60(5):563-7. doi: 10.1007/s40262-021-00987-2, PMID 33651328.
61. Hosseini A, Shorofi SA, Davoodi A. Starting dose calculation for medicinal plants in animal studies; recommendation of a simple and reliable method. Res J Pharmacogn. 2018;5:1-7.
62. Zou P, YU Y, Zheng N, Yang Y, Paholak HJ, YU LX. Applications of human pharmacokinetic prediction in first in human dose estimation. AAPS J. 2012;14(2):262-81. doi: 10.1208/s12248-012-9332-y, PMID 22407287.
63. Hemanth A, Abdul HA, Devanna N. Evaluating the best polyethylene glycol as solid dispersion carrier by taking etoricoxib as a model drug. Asian J Pharm Clin Res. 2019;12(3):250-5. doi: 10.22159/ajpcr.2019.v12i3.30251.
64. Limongi T, Susa F, Allione M, DI Fabrizio E. Drug delivery applications of three dimensional printed (3DP) mesoporous scaffolds. Pharmaceutics. 2020;12(9):851. doi: 10.3390/pharmaceutics12090851, PMID 32911620.
65. Akila RM, Janani M. Development characterization and evaluation of the antimicrobial properties of biodegradable porous scaffolds loaded with natural vanillin. Int J Pharm Pharm Sci. 2023;15(11):31-7. doi: 10.22159/ijpps.2023v15i11.48987.
66. Soni G, Yadav KS, Gupta MK. QBD based approach for formulation development of spray-dried microparticles of erlotinib hydrochloride for sustained release. J Drug Deliv Sci Technol. 2020;57:101684. doi: 10.1016/j.jddst.2020.101684.
67. Javed MN, Kohli K, Amin S. Risk assessment integrated QBD approach for development of optimized bicontinuous mucoadhesive limicubes for oral delivery of rosuvastatin. AAPS Pharm Sci Tech. 2018;19(3):1377-91. doi: 10.1208/s12249-018-0951-1, PMID 29388027.
68. Ali R, Mehta P, Kyriaki Monou PK, Arshad MS, Panteris E, Rasekh M. Electrospinning/electrospraying coatings for metal microneedles: a design of experiments (DOE) and quality by design (QBD) approach. Eur J Pharm Biopharm. 2020;156:20-39. doi: 10.1016/j.ejpb.2020.08.023, PMID 32871196.
69. AW MS, Khalid KA, Gulati K, Atkins GJ, Pivonka P, Findlay DM. Characterization of drug release kinetics in trabecular bone from titania nanotube implants. Int J Nanomedicine. 2012;7:4883-92. doi: 10.2147/IJN.S33655, PMID 23028217.
70. Dhas SK, Deshmukh G. Formulation and evaluation of meloxicam microspheres for colon targeted drug delivery. Asian J Pharm Clin Res. 2021;14(8):45-51. doi: 10.22159/ajpcr.2021.v14i8.38482.
71. Gobin AS, Butler CE, Mathur AB. Repair and regeneration of the abdominal wall musculofascial defect using silk fibroin chitosan blend. Tissue Eng. 2006;12(12):3383-94. doi: 10.1089/ten.2006.12.3383, PMID 17518675.
72. Gulati K, AW MS, Findlay D, Losic D. Local drug delivery to the bone by drug-releasing implants: perspectives of nano-engineered titania nanotube arrays. Ther Deliv. 2012;3(7):857-73. doi: 10.4155/tde.12.66, PMID 22900467.
73. Dominas C, Deans K, Packard R, Jonas O. Preparation and sterilization of an implantable drug delivery microdevice for clinical use. MethodsX. 2021;8:101382. doi: 10.1016/j.mex.2021.101382, PMID 34430278.
74. Stewart SA, Dominguez Robles J, Donnelly RF, Larraneta E. Implantable polymeric drug delivery devices: classification manufacture materials and clinical applications. Polymers. 2018;10(12):1379. doi: 10.3390/polym10121379, PMID 30961303.
75. Patel RB, Solorio L, WU H, Krupka T, Exner AA. Effect of injection site on in situ implant formation and drug release *in vivo*. J Control Release. 2010;147(3):350-8. doi: 10.1016/j.jconrel.2010.08.020, PMID 20728486.
76. Rahman S, Gulati K, Kogawa M, Atkins GJ, Pivonka P, Findlay DM. Drug diffusion integration and stability of nanoengineered drug-releasing implants in bone ex-vivo. J Biomed Mater Res A. 2016;104(3):714-25. doi: 10.1002/jbm.a.35595, PMID 26481558.
77. Abpeikar Z, Milan PB, Moradi L, Anjomshoa M, Asadpour S. Influence of pore sizes in 3D-scaffolds on mechanical properties of scaffolds and survival distribution and proliferation of human chondrocytes. Mech Adv Mater Struct. 2022;29(26):4911-22. doi: 10.1080/15376494.2021.1943077.
78. LI P, Zhang W, Spintzyk S, Schweizer E, Krajewski S, Alexander D. Impact of sterilization treatments on biodegradability and cytocompatibility of zinc-based implant materials. Mater Sci Eng C Mater Biol Appl. 2021;130:112430. doi: 10.1016/j.msec.2021.112430, PMID 34702515.
79. Yadav A, Yadav M, Yadav AK, Mishra S, Jena J, Rai JK. 3D printing technique: a review on the applications in pharmaceutical manufacturing. Int J Pharm Pharm Sci. 2024;16(4):11-7. doi: 10.22159/ijpps.2024v16i4.50139.